Submitted, accepted and published by
Chemical Engineering Journal 233 (2013) 56–69

Assessment of technological solutions for improving chemical looping combustion of solid fuels with CO_2 capture

P. Gayán, Alberto Abad*, L.F. de Diego, F. García-Labiano, J. Adánez

Instituto de Carboquímica (ICB-CSIC), Dept. of Energy & Environment, Miguel Luesma Castán 4, 50018-Zaragoza, Spain.

* Corresponding author: Tel.: +34 976 733 977; fax: +34 976 733 318.

E-mail addresses: abad@icb.csic.es (A. Abad); pgayan@icb.csic.es (P. Gayán); ldediego@carbon.icb.csic.es (L.F. de Diego); glabiano@icb.csic.es (F. García-Labiano); jadanez@icb.csic.es (J. Adánez).

Abstract

The chemical looping combustion of solid fuels by *in-situ* gasification (*i*G-CLC) has great potential to reduce the economical and energetic cost of CO_2 capture for generating energy from coal. Previous studies have highlighted that a high CO_2 capture rate can be reached, but incomplete combustion is predicted by theoretical models or obtained during experimental work. In this paper, a mathematical model for the fuel reactor and carbon stripper, validated through experimental results, is adapted to evaluate the relevance of several technological improvements in order to increase the combustion efficiency of the *i*G-CLC process. The technological options evaluated include increasing the gas-solid contact in the fuel reactor, incorporating a secondary fuel reactor, re-circulating exhaust gases to the fuel reactor or the carbon stripper, or feeding coal into the carbon stripper instead in the fuel reactor. Model simulations showed that the use of a secondary fuel reactor has the major impact by reducing the unburnt compounds in the CO_2 stream. The origin of the unburnt compounds is determined from a thorough analysis of the results obtained during the evaluation of these technological options. Thus, a new arrangement of the *i*G-CLC reactors is proposed, one which would minimise the presence of

unburnt compounds. In this concept, exhaust gases from the fuel reactor are sent to the carbon stripper. The oxygen demand for this concept is predicted to be $\Omega_T = 0.9\%$.

Keywords: CO_2 capture; Chemical-looping combustion; Coal; Simulation; Optimisation.

Highlights

- Several technological options to improve the performance of *i*G-CLC are analysed.
- A mathematical model is developed to evaluate the performance of each option.
- The use of a secondary fuel reactor increases the potential to reduce the oxygen demand.
- A new *i*G-CLC configuration is proposed which minimises oxygen demand.

1. Introduction

Chemical looping combustion (CLC) is one of the most promising combustion technologies for carrying out CO_2 capture with low economic and energetic costs [1]. The CLC process is based on the transfer of oxygen from air to the fuel by means of a solid oxygen carrier, avoiding direct contact between the fuel and air. Ideally, the CO_2 capture is inherent in this process. In recent years there has been growing interest in the use of CLC in the CO_2 capture from coal combustion [2]. Fig. 1 shows a general diagram of a CLC system using coal as fuel, based on the configuration existing in the 1 MW_{th} CLC unit at Technische Universität Darmstadt [3]. A CLC system is largely composed of two reactors, namely an air and a fuel reactor, with the oxygen carrier circulating between them. In *in-situ* gasification chemical looping combustion (*i*G-CLC), coal is fed into the fuel reactor. The *in-situ* gasification of coal occurs here, see reaction (1-3), as well as the subsequent oxidation of the gases generated by the reaction with the oxygen carrier (Me_xO_y), see reactions (4-6). The water-gas shift (WGS) reaction can have also some significance in the product distribution, see reaction (7). The reduced oxygen carrier (Me_xO_{y-1}) is transferred to the air reactor where it is regenerated with air, see reaction (8), to be later transferred to the fuel reactor.

Submitted, accepted and published by
Chemical Engineering Journal 233 (2013) 56–69

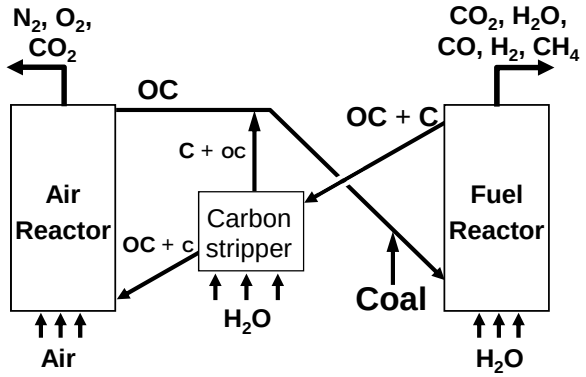

Fig. 1. Simplified flow diagram of the 1 MW_{th} CLC unit at Technische Universität Darmstadt (TUD) [3].

$$\text{Coal (s)} \rightarrow \text{H}_2\text{O (g)} + \text{Volatile matter (g)} + \text{Char (s)} \quad (1)$$

$$\text{Char (s)} + \text{H}_2\text{O (g)} \rightarrow \text{H}_2\text{ (g)} + \text{CO (g)} + \text{ash (s)} \quad (2)$$

$$\text{Char (s)} + \text{CO}_2\text{ (g)} \rightarrow 2\,\text{CO (g)} + \text{ash (s)} \quad (3)$$

$$\text{CH}_4\text{ (g)} + 4\,\text{Me}_x\text{O}_y\text{ (s)} \rightarrow \text{CO}_2\text{ (g)} + 2\,\text{H}_2\text{O (g)} + 3\,\text{Me}_x\text{O}_{y-1}\text{ (s)} \quad (4)$$

$$\text{CO (g)} + \text{Me}_x\text{O}_y\text{ (s)} \rightarrow \text{CO}_2\text{ (g)} + \text{Me}_x\text{O}_{y-1}\text{ (s)} \quad (5)$$

$$\text{H}_2\text{ (g)} + \text{Me}_x\text{O}_y\text{ (s)} \rightarrow \text{H}_2\text{O (g)} + \text{Me}_x\text{O}_{y-1}\text{ (s)} \quad (6)$$

$$\text{CO (g)} + \text{H}_2\text{O (g)} \rightarrow \text{CO}_2\text{ (g)} + \text{H}_2\text{ (s)} \quad (7)$$

$$\text{Me}_x\text{O}_{y-1}\text{ (s)} + 0.5\,\text{O}_2\text{ (g)} \rightarrow \text{Me}_x\text{O}_y\text{ (s)} \quad (8)$$

$$\text{Char (s)} + 0.5\,\text{O}_2\text{ (g)} \rightarrow \text{CO}_2\text{ (g)} + \text{ash (s)} \quad (9)$$

In *i*G-CLC , the efficiency of CO_2 capture can be reduced if char particles are by-passed to the air reactor together with the oxygen carrier stream, where they will be burnt and some CO_2 will be mixed together with the N_2 from the air; see reaction (9). A carbon separation system is used to reduce or avoid the presence of char particles in the oxygen carrier stream circulated to the air reactor, thus preventing char particles from reaching the air reactor. The carbon separation system can be based on char segregation in the fuel reactor [4,5], or segregation in an intermediate step and then re-circulation of the

char to the fuel reactor [3,6-8]. For this latter option, the separation of the char from oxygen carrier particles in a carbon stripper has been proposed [9], where char particles are separated from oxygen carrier particles through their differences in fluid dynamic properties.

The complete combustion of products generated in the fuel reactor is desired. The presence of unburnt compounds in the CO_2 stream reduces the energetic efficiency of the CLC process because some chemical energy in the fuel is not released and the energy required in the CO_2 gas processing unit (GPU) is therefore higher. The purity of the CO_2 stream after GPU may also be compromised [10]. The use of a post-combustion process downstream of the fuel reactor has been revealed as an option to overcome the presence of unburnt compounds in the CO_2 stream. However, in this case highly pure oxygen must be used as an oxidiser in order to maintain a concentrated CO_2 stream after this so-called oxygen polishing step [6]. Of course, the use of pure oxygen in this polishing step represents an energy penalty for the overall process.

Several research groups have reached important advances on the experimental demonstration of this technology in plants ranging from 1 to 100 kW_{th}. Table 1 summarises selected data for CLC with solid fuels carried out in different facilities and under experimental conditions. To evaluate the performance of a CLC unit with solid fuels, it would be desirable to know the fraction of fuel that is converted and burnt in the fuel reactor. This evaluation can be carried out by analysing the fraction of unburnt fuel exiting the fuel reactor both in gaseous and solids forms.

Submitted, accepted and published by
Chemical Engineering Journal 233 (2013) 56–69

Table 1. Experimental conditions for CO_2 capture efficiency and oxygen demand during the continuous operation of different *i*G-CLC units with different oxygen carriers.

Number	Oxygen carrier	Solid fuel	Fuel reactor	Coal feeding	Power (kW_{th})	m_{OC} (kg/MW_{th})	T (ºC)	P (atm)	CSS[(a)]	Ω_T (%)	η_{CC} (%)	$f_{C,elut}$ (%)	Ref.
1	Ilmenite	Bit. coal	Bubbling	Upper-bed	1.7	2940	950	1	yes	11.0	96	~20	[6]
2	Ilmenite	Bit. coal	Bubbling	Upper-bed	2.7	1850	950	1	yes	12.8	94	~20	[6]
3	Ilmenite	Petcoke	Bubbling	Upper-bed	4.2	1430	950	1	yes	17.3	79	n.a.	[11]
4	Ilmenite	Petcoke	Bubbling	Upper-bed	4.2	1430	1000	1	yes	15.8	86	n.a.	[11]
5	Ilmenite	Petcoke	Bubbling	Upper-bed	5.8	1030	950	1	yes	16.0	75	~28	[12]
6	Ilmenite	Petcoke	Bubbling	Upper-bed	5.8	1030	950	1	yes	18.9	83	~40	[13]
7	Ilmenite	Petcoke	Bubbling	Upper-bed	5.8	1030	1000	1	yes	19.4	87	~35	[13]
8	Ilm.+$CaCO_3$	Petcoke	Bubbling	Upper-bed	4.2	1430	1000	1	yes	15.7	86	n.a.	[11]
9	Ilm.+$CaCO_3$	Petcoke	Bubbling	Upper-bed	4.2	1430	950	1	yes	14.4	79	n.a.	[11]
10	Ilm.+$CaCO_3$	Petcoke	Bubbling	Upper-bed	9.3	645	950	1	yes	19.8	42	n.a.	[11]
11	Ilmenite	Lignite	Bubbling	In-bed	0.5	1780	920	1	no	7.0	93	7	[14]
12	Ilmenite	Bit. coal	Bubbling	In-bed	0.3	3200	940	1	no	5.0	85	5	[15]
13	Ilmenite	Bit. coal	Bubbling	In-bed	0.5	1580	890	1	no	9.0	57	5	[14]
14	Ilmenite	Bit. coal	Bubbling	In-bed	0.6	1380	920	1	no	9.0	55	5	[14]
15	Ilmenite	Bit. coal	Bubbling	In-bed	1.0	820	940	1	no	8.8	75	5	[16]
16	Ilmenite	Bit. coal	Bubbling	In-bed	3.8	1580	970	1	yes	13.1	95	~50	[17]
17	Ilmenite	Bit. coal	Bubbling	In-bed	5.6	1070	970	1	yes	11.9	92	~50	[17]
18	Ilmenite	Bit. coal	High-vel.	In-bed	87	480	963	1	yes	10.2	97	47	[7,18]
19	Ilmenite	Bit. coal	High-vel.	In-bed	34	280	932	1	yes	14.0	88	n.a.	[7]
20	Ilmenite	Bit. coal	High-vel.	In-bed	137	144	931	1	yes	12.2	96	n.a.	[7]
21	Ilmenite	Bit. coal	High-vel.	In-bed	204	87	931	1	yes	15.4	92	n.a.	[7]
22	Ilmenite	Anthracite	Bubbling	In-bed	0.6	1400	920	1	no	3.8	40	10	[14]
23	Ilmenite	Petcoke	Bubbling	In-bed	5.7	1050	970	1	yes	8.6	87	~50	[17]
24	Ilmenite	Petcoke	Bubbling	In-bed	9.0	670	970	1	yes	9.6	70	~50	[17]
25	Ilmenite	Petcoke	High-vel.	In-bed	100	105	926	1	yes	8.4	78	n.a.	[19]
26	Ilmenite	Lignite	2 reactors	In-bed	12	5200	900	1	yes	10.0	95	~5	[5]
27	Ilmenite	Lignite	2 reactors	In-bed	25	2600	900	1	yes	19.2	98	~5	[5]

28	Fe_2O_3	Biomass	Spouted	In-bed	12	660	920	1	yes	14.5	95	n.a.	[20]
29	Iron ore	Biomass	Bubbling	In-bed	0.5	1400	890	1	no	10.6	97	n.a.	[21]
30	Iron ore	Biomass	Bubbling	In-bed	0.5	1400	915	1	no	3.8	98	n.a.	[21]
31	Iron ore	Bit. coal	Spouted	In-bed	0.5	1850	900	1	yes	5.0	75	n.a.	[22]
32	Iron ore	Bit. coal	Spouted	In-bed	0.5	1850	950	1	yes	4.0	85	n.a.	[22]
33	Iron ore	Bit. coal	Spouted	In-bed	0.7	1350	900	1	yes	7.3	95	n.a.	[22]
34	Iron ore	Bit. coal	Spouted	In-bed	0.7	1350	950	1	yes	5.0	97	n.a.	[22]
35	Iron ore	Bit. coal	Spouted	In-bed	0.8	1280	970	1	yes	6.2	87	n.a.	[23]
36	Iron ore	Anthracite	Spouted	In-bed	1.0	1000	970	1	yes	5.5	70	n.a.	[23]
37	Iron ore	Bit. coal	High-vel.	In-bed	51	80	950	1	no	7.2	94	~4	[24]
38	Iron ore	Bit. coal	High-vel.	In-bed	51	150	950	3	no	5.0	96	~4	[24]
39	Iron ore	Bit. coal	High-vel.	In-bed	51	180	950	5	no	4.5	98	~4	[24]
40	Fe-ESF	Bit. coal	Bubbling	In-bed	0.3	4200	940	1	no	3.0	70	n.a.	[25]
41	Fe-ESF	Bit. coal	Bubbling	In-bed	0.4	2730	930	1	no	6.0	68	n.a.	[26]
42	Fe-ESF	Bit. coal	Bubbling	In-bed	1.0	1200	905	1	no	6.0	65	n.a.	[25]
43	Fe-ESF	Anthracite	Bubbling	In-bed	0.6	2000	930	1	no	5.0	20	n.a.	[27]
44	Manganese ore	Petcoke	Bubbling	In-bed	4.0	1500	970	1	yes	7.6	92	~35	[17]
45	Manganese ore	Petcoke	Bubbling	In-bed	5.9	1020	970	1	yes	8.6	97	~35	[17]
46	BMP	Bit. coal	Bubbling	In-bed	1.0	10000	890	1	yes	1.9	96	n.a.	[8]
47	$NiO/NiAl_2O_4$	Bit. coal	Spouted	In-bed	0.7	1450	980	1	yes	3.5	95	~8	[28]
48	$NiO/NiAl_2O_4$	Bit. coal	Spouted	In-bed	8.3	965	960	1	yes	4.1	78	8	[4]
49	$NiO/NiAl_2O_4$[(b)]	Bit. coal	Spouted	In-bed	8.3	965	960	1	yes	17.6	n.a.	n.a.	[29]
50	$CuO/MgAl_2O_4$	Biomass	Bubbling	In-bed	1.2	625	935	1	no	0.0	100	<5	[30]
51	$CuO/MgAl_2O_4$	Lignite	Bubbling	In-bed	0.6	845	940	1	no	0.0	99	~0	[31]
52	$CuO/MgAl_2O_4$	Bit. coal	Bubbling	In-bed	0.6	1000	940	1	no	0.0	99	~0	[31]
53	$CuO/MgAl_2O_4$	Bit. coal	Bubbling	In-bed	0.8	710	940	1	no	0.0	90	~0	[31]
54	$CuO/MgAl_2O_4$	Bit. coal	Bubbling	In-bed	1.5	240	940	1	no	0.0	99	~0	[32]
55	$CuO/MgAl_2O_4$	Anthracite	Bubbling	In-bed	0.6	895	940	1	no	0.0	85	~0	[31]

[(a)] Shows whether or not a carbon separation system (CSS) was present
[(b)] Deactivated material

On the one hand, H_2, CO and CH_4 are the main unconverted compounds in the gases [15]. Considering the oxygen polishing step as a solution, the total oxygen demand, Ω_T, is often used to evaluate the fraction of unconverted gaseous compounds. The oxygen demand is defined as the fraction of stoichiometric oxygen required to fully oxidise the unconverted gases exiting the fuel reactor to CO_2 and H_2O with respect the stoichiometric oxygen demand of the fuel:

$$\Omega_T = M_O \frac{(F_{H_2} + F_{CO} + 4F_{CH_4})_{FR,out}}{\Omega_{coal}\dot{m}_{coal}} \quad (10)$$

In this study, sulphur and nitrogen compounds coming from S and N in coal are not considered in the oxygen demand because it has been demonstrated that in the *i*G-CLC process most of sulphur occurs in the form of SO_2 and most of nitrogen is in the form of N_2 [23].

On the other hand, unconverted solid fuel is usually found as carbon in char particles either going to the air reactor or being elutriated from the fuel reactor and exiting together with the gaseous stream. Carbon entering into the air reactor is evaluated through the CO_2 capture efficiency, η_{CC}, defined as the carbon in coal the fed minus carbon (mostly CO_2) at the air reactor exit divided by the carbon in the coal fed. The other source of solid carbon losses is in elutriated char particles, which can be evaluated through the fraction of carbon in the coal fed which is actually elutriated and exits in the gaseous stream from the fuel reactor, denoted as $f_{C,elut}$.

In some cases, the combustion efficiency in FR, $\eta_{c,FR}$, is given as an additional parameter to evaluate the performance of an oxygen carrier in the CLC process with solid fuels [14-16,25,26]. $\eta_{c,FR}$ is defined as the oxygen required to fully oxidise unconverted gaseous compounds divided by the oxygen required to burn coal converted in the fuel reactor, i.e. the coal fed minus both the char elutriated and the char sent to the air reactor. Thus, $\eta_{c,FR} = 1 - \Omega_{OD,}$ with Ω_{OD} being the oxygen demand in the fuel reactor as defined in other studies found in the literature [6,7,11-13,17]. However, Ω_T, η_{CC} and $f_{C,elut}$ are necessary and sufficient to evaluate the system. For example, Ω_{OD} can be deduced as a function of Ω_T, η_{CC} and $f_{C,elut}$:

$$\Omega_{OD} = \Omega_T \frac{\Omega_{coal}}{\Omega_{coal} - f_{C,elut} f_{C,fix} \frac{M_{O_2}}{M_C} - (1-\eta_{CC}) f_C \frac{M_{O_2}}{M_C}} \quad (11)$$

Table 1 summarises the oxygen demand, Ω_T, CO_2 capture efficiency, η_{CC}, and the fraction of elutriated carbon, $f_{C,elut}$, are summarised for different solids inventories, oxygen carrier materials and solid fuel types. In the case where these parameters were not available in the sources, the value shown has been estimated from the results shown in the article in question. For example, Ω_T has been deduced from Ω_{OD} values or $f_{C,elut}$ from the solid fuel conversion, η_{SF}, defined as the ratio between the total flow of gaseous carbon leaving the CLC unit and the total flow of carbon fed to the system with the coal [6,7,11-13,17]. In other cases, a direct calculation from the concentration of gases at the fuel and/or air reactor exit was carried out. In these cases, there may be some uncertainty with respect to the exact values of these parameters, but in general it is possible to evaluate the oxygen demand trend.

In these studies, a high CO_2 capture can be accomplished by using high temperatures, high amounts of solids in the fuel reactor –which increases the residence time of particles-, highly reactive solid fuels and/or implementing a carbon separation system. A simulation of results showed the importance of the carbon separation system efficiency for obtaining a high value of CO_2 capture without a high amount of solids in the fuel reactor [18-33-34]. In fact, a highly efficient carbon stripper has been identified as the main factor responsible for obtaining high CO_2 capture efficiencies in a 100 kW_{th} CLC unit [18]. The oxygen carrier used was less important in the CO_2 capture obtained. The fraction of char elutriated from the fuel reactor is reported or can be calculated only in some cases. Values lower than 5% were reported for a bubbling fluidised fuel reactor, but values as high as 50% were found in high-velocity fluidisation mode because of insufficient performance of the cyclone downstream from the fuel reactor.

The complete combustion of gases was not reached in the fuel reactor during the CLC of coal in *i*G-CLC mode. Thus, total oxygen demand values between 2 and 20% are reported. The fraction of elutriated carbon from the fuel reactor does not contribute to Ω_T, as it is defined. Thus, if the CLC system was improved by increasing η_{CC} or decreasing $f_{C,elut}$, an increase in Ω_T in certain cases may be expected, depending on the origin of the unburnt compounds. Take for example two extreme cases: firstly, an accumulation of gasification products (CO and H_2) in the freeboard is highly relevant when

the fuel reactor is operating in high-velocity fluidisation mode [29-31], where $f_{C,elut} \approx 50\%$. In this case, if char particles were fully recovered by the cyclone and recycled to the fuel reactor, then the total oxygen demand could be doubled [18]. If this is not the case, the incomplete combustion of volatile matter is the main factor responsible for the appearance of unconverted gases (mainly H_2, CO and CH_4) when the fuel reactor is in bubbling fluidisation mode [15]. In these cases, the total oxygen demand would not vary with η_{CC} or $f_{C,elut}$. Therefore, besides Ω_T, η_{CC} and $f_{C,char}$, it is very interesting to find out the origin of any unburnt compounds. Simulation using a validated model is a powerful tool to identify these origins [18].

Unconverted gases must be processed before the CO_2 transportation and sequestration. Fig. 2 shows the values of oxygen demand obtained in different CLC units operating with a variety of oxygen carrier materials and solid fuels. It highlights the impact of the gas-solid contact, the type of solid fuel, the oxygen carrier material and the solids inventory on oxygen demand. Although temperature also has an influence on oxygen demand, its impact is of lesser importance [18,35]. Some tests carried out under pressurised conditions revealed the positive influence of pressure [24].Oxygen demand is high when the volatile matter has a low level of contact with oxygen carrier particles [5,6,11-13], suggesting the importance of volatile matter conversion on combustion efficiency. Solid fuels with a highly volatile matter fraction (e.g. biomass or lignite) therefore usually show higher oxygen demand values than solid fuels with a low volatile matter fraction (e.g. anthracite and petcoke) [14]. Most of the experimental work has been carried out using Norwegian ilmenite as an oxygen carrier, with oxygen demand values of between 5-15%. However, oxygen carrier reactivity has also a great influence on oxygen demand. Thus, more reactive oxygen carriers (e.g. Fe-ESF, iron ore or Ni-based materials) give lower oxygen demand values. This effect is highlighted when a Ni-based material is deactivated, and, as a consequence, a much higher oxygen demand value is obtained [29]. Nevertheless, a loss of oxygen carrier particles mixed with ash particles is expected, so expensive and/or environmental unfriendly materials, such as Ni-based materials, are less preferable for CLC processes with solid fuels.

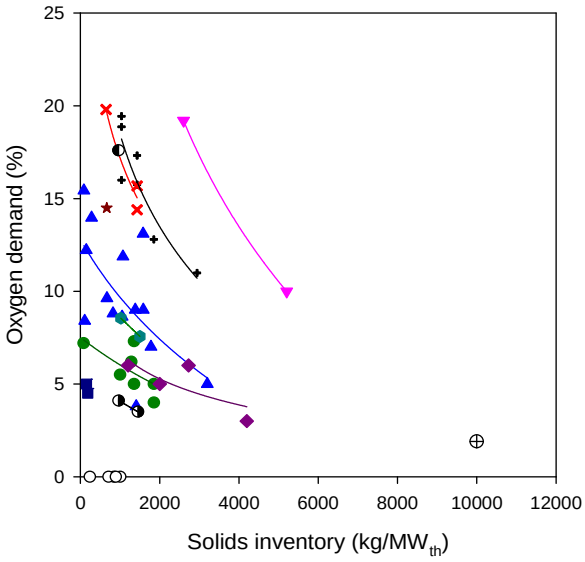

Fig. 2. Oxygen demand reported or calculated from data found in the literature as a function of the fuel reactor solids inventory in the *i*G-CLC process. Symbol points in Table 1: points 1-7: ✚ (ilmenite); points 8-10 ✖ (ilmenite+limestone); points 11-25: ▲ (ilmenite); points 26-27: ▼ (ilmenite); point 28: ★ (Fe_2O_3); points 29-37: ● (iron ore); points 38-39: ■ (iron ore); points 40-43: ◆ (Fe-ESF); points 44-45: ⬢ (manganese ore); point 46: ⊕ (BMP); points 47-48: ◑ ($NiO/NiAl_2O_4$); point 49: ◐ (deactivated $NiO/NiAl_2O_4$); points 50-55: ○ ($CuO/MgAl_2O_4$ in CLOU mode).

Unburnt compounds are generally always present in the gaseous stream from the fuel reactor, except when Cu-based materials are used [30-32]. The complete combustion obtained with Cu-based materials is not related to the high reactivity of this material [36,37], but rather to a different mechanism occurring during coal conversion. CuO has the ability to break down into Cu_2O and O_2 at high temperatures. The advantage of this property is harnessed in the so-called chemical looping with oxygen uncoupling process (CLOU) proposed by Mattisson et al. [38]. So, coal can be burnt with oxygen released in the fuel reactor by the oxygen carrier, with the coal conversion in CLOU being more efficient than during the *in-situ* gasification of coal.

Finally, there is a clear trend visible for oxygen demand to fall as the solids inventory in the fuel reactor increases. However, unburnt compounds are expected to be present in the *i*G-CLC process, regardless of the oxygen carrier used or the operational conditions. If you want to reduce the oxygen demand of exhaust gases, additional actions should be taken. These actions may include the following operational options:

O-1. Modifying certain operational conditions with a beneficial effect on the combustion efficiency in the fuel reactor. In this way, an increase in the fuel reactor temperature or pressure, or an increase in the solids inventory or circulation flow rate could improve the combustion efficiency of the process. A less significant impact is expected by varying the steam to coal ratio or the coal particle size [18,35]. Sozinho et al. [8] showed that oxygen demand was low (Ω_T = 1.9%) but not zero when the oxygen carrier inventory was high (estimated to be 10000 kg/MW_{th} of the BMP material), which is congruent with theoretical predictions [39]. Nevertheless, a low reduction in oxygen demand is expected if the solids inventory is increased above 1000-2000 kg per MW_{th} [35,39]. If the char conversion is low, an increase in the temperature may lead to an increase in oxygen demand because the oxygen carrier must oxidise a higher fraction of fuel converted in the fuel reactor [35]. Nevertheless, a high char conversion is required in order to obtain a high level of CO_2 capture, which requires the use of a carbon separation system. In this case, an increase in the temperature reduces oxygen demand [18]. An increase in the solids circulation rate has a significant effect, decreasing the oxygen demand in the oxygen carrier to fuel ratios ϕ_{OC} <5; however, high ϕ_{OC} values are not recommended because the loss in CO_2 capture is too high [18]. Previous studies showed that optimal operational conditions consisted of a temperature between 1000-1100ºC, an oxygen carrier to fuel ratio in the range of ϕ_{OC} = 1.2-5 and a solids inventory within the region of 1000-2000 kg/MW_{th} [18,35].

O-2. Using highly reactive oxygen carriers. The more reactive the oxygen carrier material, the lower the oxygen demand. However, complete combustion has not been achieved even for highly reactive materials. This issue was analysed in a previous study, showing that very high reactivity changes would be necessary to decrease the oxygen demand to values close to zero [35]. Moreover, the

choice of material as an oxygen carrier for *i*G-CLC must take into account other factors, such as its cost, environmental impact and durability. Materials with oxygen uncoupling properties may be preferable because of their superior performance during the CLOU process. However, these materials are synthetic and generally more expensive than materials used for *i*G-CLC, and processes to recover active materials lost together with spent ash particles would need to be adopted.

Other options are related to design modifications, which alter the configuration of the *i*G-CLC system in some way, see Fig. 3:

D-1. Improving the gas-solid contact by placing geometrical constrictions or internals in the dilute region of the fuel reactor. This solution has been proposed in the literature to increase the amount of solids in the dilute region, thus making the gas-solid contact in this zone more effective [40,41].

D-2. Including a secondary fuel reactor fed by the exhaust gases. In this secondary reactor, the oxidation of unburnt compounds will occur. This concept was adopted in a 25 kW_{th} unit at Technische Universität Hamburg [5].

D-3. Recycling exhaust gas to the fuel reactor [10] or carbon stripper. Although oxygen demand would be reduced, some unburnt compounds are expected to remain in the flue gases because of the intrinsic limitation when re-circulated stream gases are used. Gas recycling needs more components, however lower oxygen requirements are expected.

D-4. Unburnt compounds separated during the CO_2 purification and compression step can be returned to the fuel reactor. Recycling to the fuel reactor requires the extraction of a purge stream to avoid N_2 accumulation from coal in the system, which can result in a loss in CO_2 capture.

D-5. Feeding coal into the carbon stripper. In this case, the carbon stripper also acts as a primary fuel reactor. The original fuel reactor can now be viewed as a secondary fuel reactor with a cross-current of gases and solids.

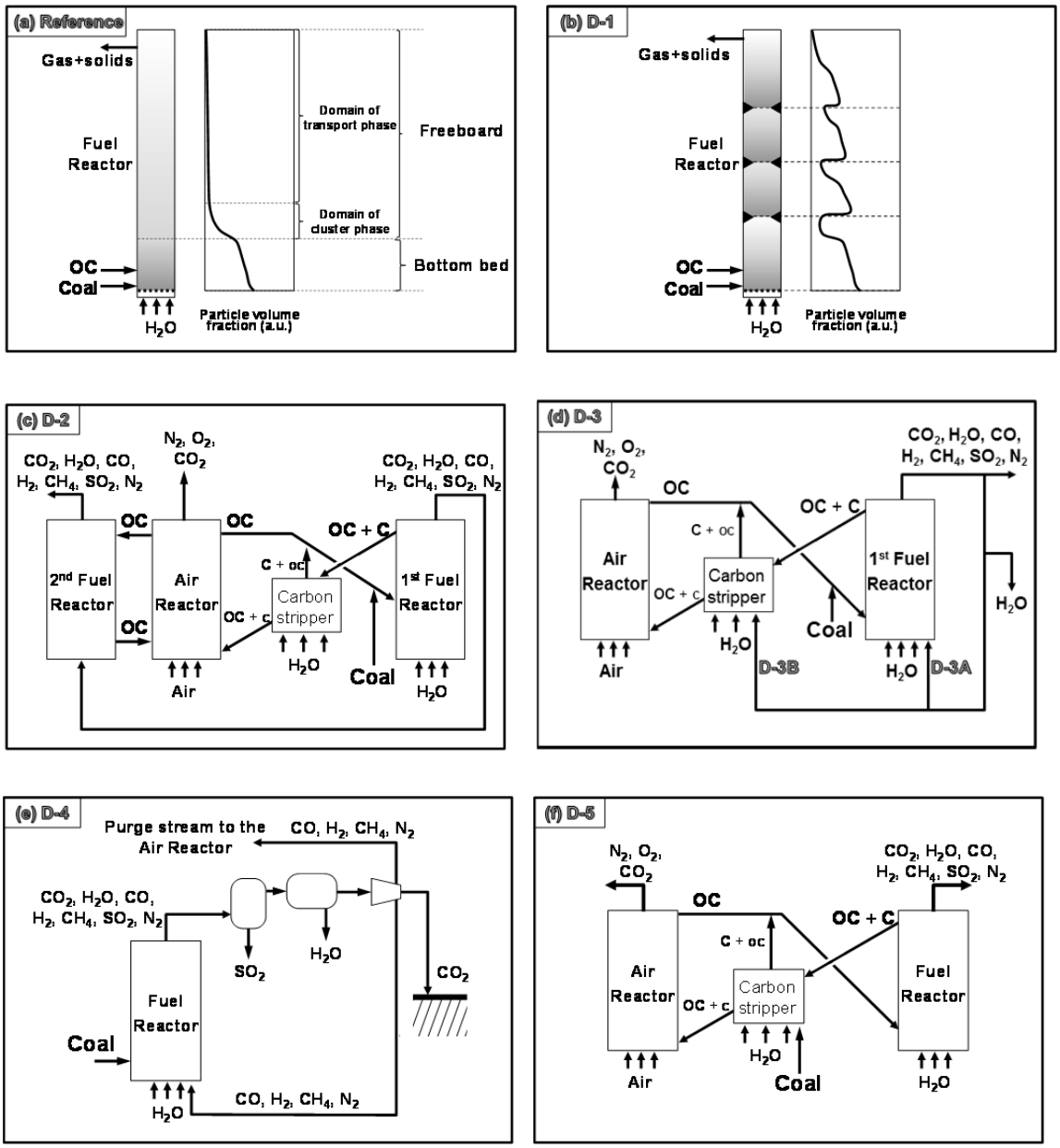

Fig. 3. Diagrams of the different configurations for the improvement of the *i*G-CLC process implementing different technological options.

The objective of this study is to evaluate the potential of several technological options to reduce the oxygen demand needed for the oxygen polishing step in the *i*G-CLC process. The composition of gases exiting the CLC system is predicted using a model previously developed for the fuel reactor [34,35]. This model was validated against experimental results obtained in a 100 kW_{th} CLC unit using coal [18]. The model here is modified to incorporate the different options described in D-1 to D-5. The results are presented in order to find out the composition of the gas reaching the GPU and then evaluated to identify the technological options with a the most potential to reduce or to even remove the oxygen requirements for the oxygen polishing step in a *i*G-CLC process. The CO_2 capture efficiency for each option is also predicted. The results presented in this paper will be useful to estimate the energetic efficiency of the CLC process using solid fuels.

2. Working hypothesis

2.1. Background

In a previous paper, a mathematical model of the fuel reactor was presented for coal combustion in a *i*G-CLC system [34]. This model takes into account the reactor fluid dynamics, the coal conversion (devolatilisation and gasification) and the reaction of the oxygen carrier with gases evolved from coal. The fluid dynamics model has been successfully used to predict the behaviour of high-velocity fluidised bed reactors within the range of 0.1 [18] to 12 MW_{th} [42].The fuel reactor used was a fluidised bed working on high-velocity mode. It was split into two zones divided vertically with respect to axial concentration and the backmixing of solids: the bottom bed and the freeboard, see the reference example in Fig. 3. The gas flow in the bottom bed is shared between the emulsion and bubble phases, with gas mixing between them controlled by diffusion. The freeboard is composed of the cluster phase and a transport or dispersed phase. Both the cluster and transport phases are superimposed, but they have different mixing behaviours. The cluster phase has a strong solids backmixing with solids in the bottom bed, whereas the transport phase is characterised by a core/annulus flow structure with a lateral exchange of solids between them. A net flow of solids goes through the core and particle backmixing occuring at the reactor walls. A differential mass balance between the reacting and product gases (H_2,

CO, CH_4, H_2O and CO_2) is included to calculate the molar flow variation with the height of each compound inside the reactor. The reaction kinetics for oxygen carrier reduction, coal gasification and WGS reaction are considered in the mass balance following the pathway given in reactions (1-7). It was assumed that sulphur was present as SO_2 and nitrogen as N_2, since these have been identified as the major compounds at the fuel reactor exit [23,28,43]. Further information on the model is available elsewhere [18,34,35].

The fuel reactor model was developed to determine the operating conditions which optimised the CO_2 capture and combustion efficiency of the *i*G-CLC process in the 1 MW_{th} CLC unit erected at Technische Universität Darmstadt (TUD). The air reactor was not modelled, and the complete oxidation of the oxygen carrier and the combustion of possible char particles entering to the air reactor were assumed.

Later, this model was validated against experimental results obtained in a 100 kW_{th} CLC unit erected at the Chalmers University of Technology. No major modifications into the model were required to validate it [18]. The oxygen demand and CO_2 capture was predicted with an error lower than 5% with variations in the temperature (956-976ºC), pressure drop (15-23 kPa), steam flow (6-18 Nm^3/h) and solids circulation flow rate (990-3210 kg/h). The key operating parameters affecting to the behaviour of the fuel reactor were identified. Mathematical modelling of the fuel reactor in the *i*G-CLC process emerged as an important tool to identify the reasons for incomplete combustion [34,35]. Both the incomplete conversion of volatile matter -mainly CH_4 because of its low reactivity with ilmenite – and the accumulation of gasification products in the freeboard are responsible for the remaining unburnt compounds together the CO_2 stream exiting the fuel reactor.

2.2 Conditions for the reference case

The initial hypothesis for this paper was to consider the geometry of the fuel reactor and carbon stripper existing in the 1 MW_{th} CLC unit at Technische Universität Darmstadt [3], see Table 2 and Fig. 1. The oxygen carrier (OC) and ungasified carbon (C) exit the fuel reactor to the carbon stripper. Most of the carbon is separated in the carbon stripper, allowing the oxygen carrier particles to flow to the air reactor

together with a small fraction of carbon. The oxygen carrier and carbon are oxidised in the air reactor by air. Regenerated oxygen carrier, solids from carbon stripper and coal are all fed into the bottom part of the fuel reactor.

In line with results previously presented for the optimisation of the *i*G-CLC system [18,34,35], realistic operational conditions to maximise both combustion efficiency and CO_2 capture are proposed, see Table 3. The thermal power at the base conditions is 385 kW_{th}, and the solids inventory corresponded to 1000 kg/MW_{th}. Ilmenite was considered as oxygen carrier material, and the Colombian El Cerrejón bituminous coal was used as solid fuel. For ilmenite, the mean particle size is d_p = 0.250 mm and the particle density is ρ_p = 3710 kg/m^3, whereas values of d_p = 0.125 mm and ρ_p = 1100 kg/m^3 are considered for the solid fuel. Reaction kinetics for oxygen carrier reduction with H_2, CO and CH_4 and coal gasification with H_2O and CO_2 can be found elsewhere [34]. The oxygen transport capacity of ilmenite particles is R_{OC} = 4 wt.%, and the oxygen carrier to fuel ratio is ϕ_{OC}= 2. The ϕ_{OC} ratio is defined as the flow of oxygen available in circulating solids divided by the oxygen required to fully convert the fuel to CO_2 and H_2O. The carbon separation efficiency in the carbon stripper is assumed to be η_{CS} = 99%, which is similar to the value calculated for the 100 kW unit at Chalmers University of Technology during the model validation [18]. Under these conditions, the composition of the gas flow at the fuel reactor outlet is 15.68 vol.% CO_2, 80.85 vol.% H_2O, 2.09 vol.% H_2, 0.68 vol.% CO, 0.49 vol.% CH_4, 0.06 vol.% SO_2 and 0.15 vol.% N_2. Based on work by Kempkes and Kather [10], two options were evaluated to manage the fraction of unconverted fuel, i.e. H_2, CO and CH_4, in the flue gas, see Fig. 4:

PC-1: The post-combustion unit configured downstream from the fuel reactor: this option includes the oxygen polishing step. The oxygen demand parameter, Ω_T, characterises the requirements for oxygen, which is produced in an additional air separation unit (ASU). The oxygen used in the oxygen polishing step may contain small amounts of N_2 because the air separation was not optimal..

PC-2: The post-combustion within the air reactor: the incondensable gases (H_2, CO, CH_4 and N_2) are separated during the CO_2 compression step and then sent to the air reactor. Calculations showed that most of the CO_2 present in the flue gas is separated from incondensable gases, whereas the

CO_2 stream after compression may have a purity higher than 95% [10]. For preliminary estimations, this work assumed an ideal separation of CO_2 from incondensable gases, i.e. the purity of CO_2 was 100%, whereas no CO_2 was present in the incondensable gas stream.

Table 2. Geometrical parameters of the primary fuel reactor, carbon stripper and secondary fuel reactor. As reference, the geometry of the 1 MW_{th} CLC unit at Technische Universität Darmstadt was selected [3].

	Primary Fuel Reactor (FR-1)	Carbon Stripper (CS)	Secondary Fuel Reactor (FR-2)
Height, *H* (m)	11.4	1.0	10.0
Diameter or Width x Length (m)	0.4	1.0 x 0.5	0.4
Height of the solids inlet (m)	0.1	--	0.1

Table 3. Operational conditions in the base case for the primary fuel reactor, carbon stripper and secondary fuel reactor.

	Primary Fuel Reactor (FR-1)	Carbon Stripper (CS)	Secondary Fuel Reactor (FR-2)
Temperature (ºC)	1000	950	1000
Pressure at the outlet (kPa)	110	140	110
Pressure drop (kPa)	30	10	15-30
Solids inventory (kg)	385	510	190-380
Coal feeding rate (kg/h)	56	--	--
Solids circulation flow rate (kg/h)	5760	5760	660
Inlet gas flow (Nm^3/h)	77[(a)]	213[(a)]	390[(b)]

[(a)] 100 vol.% steam
[(b)] Gas exiting the primary fuel reactor

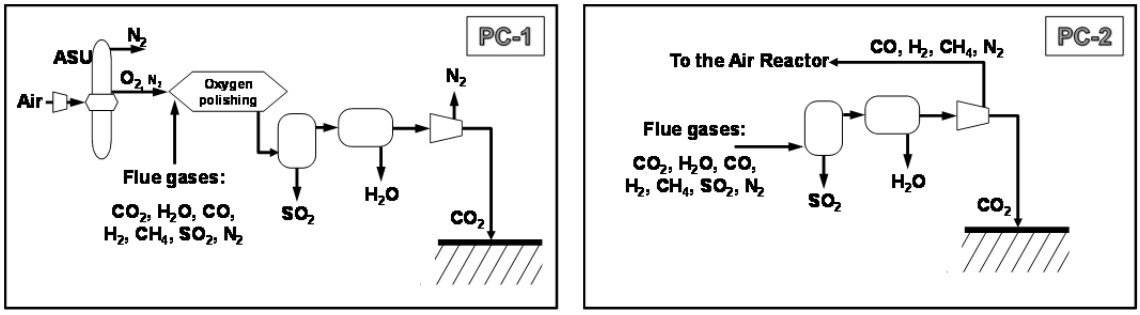

Fig. 4. General options for the post-combustion of unburnt compounds exiting the fuel reactor.

In option PC-1, the oxygen demand for the unconverted gases is $\Omega_T = 11.4\%$, whereas the CO_2 capture was predicted to be $\eta_{CC} = 96.4\%$. In option PC-2, the oxygen polishing step is avoided, so there is no

oxygen demand. However, the carbon present in the incondensable gases is sent to the air reactor, and therefore there is a loss in the CO_2 capture. Thus, the CO_2 capture efficiency for the case PC-2 is η_{CC} = 89.7%. Subsequently the potential of different design options for reducing the fraction of unconverted gases in the flue gases were analysed for both post-combustion options.

3. Results on evaluating different technological improvements to the *i*G-CLC

Previous studies have analysed the effect of several operating conditions, e.g. temperature, pressure drop, solids circulation flow rate or coal feeding rate, as well as the effect of the oxygen carrier reactivity on oxygen demand and CO_2 capture in an *i*G-CLC system [18,34]. A window for the values of these parameters was given in order to minimise oxygen demand, whereas the CO_2 capture was maintained above 95%. From these results, the operating conditions for the reference case were chosen, see section 2.2. Now, the significance of using different technological options to reduce oxygen demand is analysed. The model previously designed has been conveniently modified to encompass the design concepts for options D-1 to D-5.

3.1. D-1: Improving the gas-solid contact by incorporating geometrical constrictions

In the classical turbulent or high-velocity fluidised bed regime, the fraction of solids in the dilute region above the bottom bed is usually low, preventing the complete combustion of gases in the *i*G-CLC process, see Fig. 3(a) [34,35]. It has been shown that the presence of geometrical constrictions, e.g. in the form of ring-type internals, can extend a dense phase over the full height of the fuel reactor [40,41]. This situation is represented in Fig. 3(b). Ring-type internals produce an incremental growth in the solids concentration above the obstacle.

A preliminary estimation of the effect of the variation in solids distribution along the fuel reactor on oxygen demand is carried out by taking into account the incremental growth in solids concentration due to the presence of internals.

To consider this effect, the mathematical model previously formulated is modified in order to increase the solids concentration above the point where the internals are located in the dilute region. Thus, the solids concentration in position z^+ above the obstacle at position z is calculated by multiplying the solids concentration by the factor f_S at every axial position z where the internals are located, see Eqs. (12) and (13). Then, the solids concentration in the transport and splash (or cluster) phases above the obstacle is given by the exponential decay shown in Eqs. (14) and (15), see reference [34].

$$C_{spl}\Big|^{z^+} = f_S\, C_{spl}\Big|^{z^-} \tag{12}$$

$$C_{tr}\Big|^{z^+} = f_S\, C_{tr}\Big|^{z^-} \tag{13}$$

$$\frac{\mathrm{d}C_{spl}}{\mathrm{d}z} = -aC_{spl} \tag{14}$$

$$\frac{dC_{tr}}{dz} = -KC_{tr} \tag{15}$$

A parametric sensitivity analysis was carried out on the number of internals and the effect of every internal on increasing the solids concentration. The overall pressure drop in the reactor is maintained constant in all cases in order to analyse the effect of the different distribution of solids along the reactor but with the same amount of solids. Simulations were conducted assuming that the first internal was located at a distance Δh_{int} above the upper interphase of the bottom bed, and subsequent internals were separated by the same distance Δh_{int} until the upper part of the reactor was reached. Thus, the distance between the internals was defined by taking into account the axial positions of internals i and $i+1$:

$$\Delta h_{int} = z_{i+1} - z_i \tag{16}$$

The internal for $i = 1$ is the first one located above the bottom bed, and the rest of internals are numerically sequenced from bottom to top. The overall pressure drop in the reactor is given by the sum of the pressure drop in the bottom bed together with the pressure drop in the dilute region, see Eq. (17). As the overall pressure drop is considered to be constant, lesser solids must be located in the bottom bed since more solids are to be found in the dilute region when internals are included. As a consequence, the height of the bottom bed, H_b, is reduced.

$$\Delta P = \int_0^{H_b} C_b g dz + \int_{H_b}^{z_1} \left(C_{spl} + C_{tr}\right) g dz + \sum_1^{n_{int}} \int_{z_i}^{z_{i+1}} \left(C_{spl} + C_{tr}\right) g dz \quad (17)$$

Fig. 5 shows the oxygen demand and the CO_2 capture corresponding to the post-combustion option PC-1 predicted for different separation between internals as a function of the multiplying factor f_S. The amount of solids increases in the freeboard and decreases in the bottom bed as the f_s value increases. So, there is a maximum limit for f_s at which there should be no solids in the bottom bed in order to keep the pressure drop in the reactor constant. The limit corresponds to the end lines shown in Fig. 5. The higher the separation between internals, i.e. the higher Δh_{int} is, the higher the possible value for f_S.

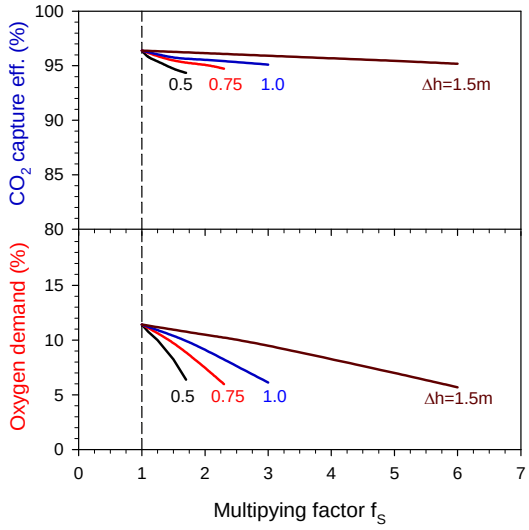

Fig. 5. Oxygen demand and CO_2 capture predicted for option D-1 combined to post-combustion PC-1: layout of internals in the dilute region and oxygen polishing. Results as a function of the separation between obstacles and the multiplying factor of the solids concentration, f_S.

Oxygen demand decreases as the f_S factor increases because a higher amount of solids is to be found above each obstacle. Likewise oxygen demand decreases as the distance between the obstacles decreases, i.e. the number of internals in the reactor is higher. In order to maintain the same pressure drop in the fuel reactor, the amount of solids in the bottom bed decreases as f_S increases or Δh_{int} falls. Here it is important to note that the bottom bed is ineffective burning the volatile matter because of the

poor gas-solid contact in this phase [34]. Hence more solids are present above every obstacle as f_S increases or Δh_{int} decreases, whereas the gas-solid contact is improved, at the expense of the amount of solids in the bottom bed decreasing. As a result, the combustion efficiency in the fuel reactor is increased and oxygen demand decreases.

Nevertheless, CO_2 capture falls a little with an increase in f_S or decrease in Δh_{int}. This slight decrease is due to an increase in the flow of solids exiting the fuel reactor, since the solids concentration at the upper part of the reactor is higher. A higher flow of unconverted carbon reaches the carbon stripper, which maintains the same carbon separation efficiency, $\eta_{CS} = 99\%$. Therefore, the CO_2 capture falls because more unconverted carbon is able to reach the air reactor.

In the post-combustion PC-2, there is no oxygen polishing step. Instead, unconverted gases (H_2, CO and CH_4) are separated from the CO_2 and sent to the air reactor. In this case, CO_2 capture slightly increases with the multiplying factor f_S as well as with a decrease in Δh_{int}. This fact is related to the improved gas conversion in the fuel reactor. Moreover, the flow of unconverted gases decreases, meaning a lower flow of carbon is sent to the air reactor, decreasing the CO_2 flow exiting the air reactor.

If a multiplying factor $f_S = 2$ is assumed to be a realistic value and internals are located every 0.75 m, values of $\Omega_T = 7.5\%$ for the oxygen demand and of $\eta_{CC} = 95.1\%$ for the CO_2 capture efficiency are obtained for post-combustion option PC-1, which can be compared with $\Omega_T = 11.4\%$ and $\eta_{CC} = 96.4\%$ in the reference case. It would be expected that a higher f_S value would bring down the oxygen demand, but the pressure drop in the reactor must be increased because the pressure drop given by the solids above the internals would be higher than the assumed value for the whole reactor, $\Delta P_{FR} = 30$ kPa. By definition, oxygen demand is zero in post-combustion option PC-2. The CO_2 capture efficiency, η_{CC}, is increased from 89.7% in the reference case to 90.7%.

3.2. D-2: Including a secondary fuel reactor fed by exhaust gases

In this option, a secondary fuel reactor is included in the configuration. Fig. 3(c) shows a general diagram of this option. Both fuel reactors are placed in parallel for solids but in a series for gases. The

solid material in the secondary reactor comprises the oxygen carrier coming from the air reactor, and it is fluidised by gases coming from the primary fuel reactor. The secondary fuel reactor is assumed to operate at high-velocity fluidisation mode, so the mathematical model for the fuel reactor is also valid. Dimensions for the secondary reactor are similar to those of the primary fuel reactor, see Table 2, and operating conditions are shown in Table 3. The gas velocity at the reactor inlet is set at 4 m/s, whereas the oxygen carrier to fuel ratio is $\phi_{OC} = 2$. The solids inventory varies from 190 to 380 kg, corresponding to 500-1000 kg/MW_{th}, by changing the pressure drop between 15 and 30 kPa. Lower solids inventory values in the secondary fuel reactor are not evaluated in order to allow for the existence of a dense zone in the bottom bed.

For the post-combustion PC-1 option, an important decrease in oxygen demand is predicted with the presence of the secondary reactor; however, a minor variation in oxygen demand is estimated when the amount of solids in this reactor is varied. Thus, oxygen demand is reduced from 11.4% to 1.7% when the solids inventory in the secondary fuel reactor is 500 kg/MW_{th}. A reduction of oxygen demand to Ω_T = 1.5 % is reached with 1000 kg/MW_{th}, i.e. Ω_T decreases a further 12% when the solids inventory is doubled. In all cases, H_2 and CO are fully converted to H_2O and CO_2, respectively. Thus, oxygen demand only corresponds to unconverted CH_4 because of its low reactivity with ilmenite [44]. Due to the small difference in oxygen demand when the solids inventory is doubled from 500 to 1000 kg/MW_{th}, it can be concluded that with the lower amount of solids, as possible in the secondary fuel reactor, it is preferable to have a pressure drop as low as possible. The CO_2 capture is maintained constant, η_{CC} = 96.4%, in all cases because the coupling formed by the primary fuel reactor and carbon stripper is not affected by the presence of the secondary reactor.

If the post-combustion PC-2 option is considered, the efficiency of the CO_2 capture increases from 89.7% to 95.5%. This means that there is only a small penalty in η_{CC} with respect to the PC-1 option. This is due to the low amount of carbon in unconverted gases after the combustion in the secondary fuel reactor.

3.3. D-3: Recycling exhaust gas

3.3.1. D-3A: Recycling exhaust gas to the fuel reactor

To improve gas conversion, a fraction of the exhaust gases from the fuel reactor can be re-circulated to the fuel reactor itself. This option is called D-3A, and dry re-circulation is assumed. Also, steam fed into the fuel reactor is replaced by re-circulated gases to reduce the steam consumption.

In the D-3A option, the same mathematical model previously explained is used without major changes. In this case, only the variation in the gas flux and composition at the fuel reactor inlet is taken into account. The results are evaluated as a function of the re-circulation ratio of gas on a dry basis, $\phi_{g,dry}$, defined as:

$$\phi_{g,dry} = \frac{F_{rec,dry}}{F_{outFR,dry}} \tag{18}$$

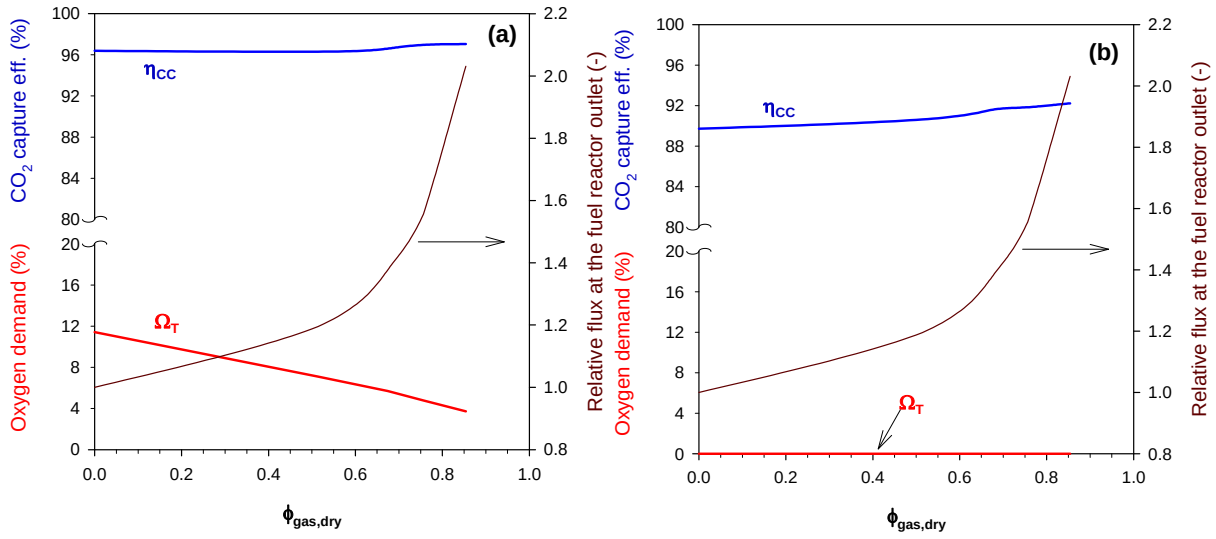

Fig. 6. Oxygen demand and CO_2 capture predicted for the technological option D-3A: dry re-circulation of exhaust gases to the fuel reactor. The results as a function of re-circulation ratio, $\phi_{g,dry}$. Post-combustion options: (a) PC-1 and (b) PC-2.

Figs. 6(a) and 6(b) show the oxygen demand and CO_2 capture efficiency predicted by the model as a function of the $\phi_{g,dry}$ ratio for the post-combustion PC-1 and PC-2 options, respectively. As expected for option PC-1, oxygen demand decreases as the gas recirculation $\phi_{g,dry}$ ratio increases. Thus, when the $\phi_{g,dry}$ ratio becomes 0.85, oxygen demand decreases to $\Omega_T = 3.7\%$ compared to the reference value, $\Omega_T = 11.4\%$. CO_2 capture is barely affected by $\phi_{g,dry}$ because conditions affecting the gasification reaction are roughly constant. This is due to the high steam concentration in the reactor, which is determined by the high steam flow fed into the carbon stripper that runs to the fuel reactor. Hydrogen concentration is also maintained at similar low levels in all cases, minimising the inhibitory effect of H_2 on char gasification. In option PC-2, CO_2 capture efficiency increases with the $\phi_{g,dry}$ ratio due to the lower flow of carbon in the incondensable gases. The CO_2 capture is $\eta_{CC} = 92.2$ % at $\phi_{g,dry} = 0.85$, which is higher than the 89.7 % shown in the reference case.

Fig. 6 also shows the relative flux of gas in the fuel reactor as a function of the $\phi_{g,dry}$ ratio. The relative flux is defined as the existing gas flow divided by the gas flow in the reference case, i.e. when gas re-circulation is not considered. It should be noted that at $\phi_{g,dry} = 0.85$ the gas flow at the fuel reactor outlet is doubled. This affects the fluid dynamics of the reactor. Thus, more solids are to be found in the dilute region at the expense of a lower amount of solids in the bottom bed. At a higher $\phi_{g,dry}$ ratio, the presence of solids in a dense bed is avoided if the total pressure drop is maintained at $\Delta P_{FR} = 30$ kPa. As a consequence, $\phi_{g,dry}$ ratios above 0.85 have not been evaluated.

Variations to the case considered here could include a wet re-circulation or the maintenance of the steam flow to the fuel reactor. Marginal differences to oxygen demand and CO_2 capture are predicted between wet or dry re-circulation when the results obtained for similar re-circulation ratios are compared. However, the ratio of re-circulated wet gases is limited to low values because a high velocity of gases at the fuel reactor inlet is soon reached. As high re-circulation ratios are suitable for reducing oxygen demand, dry re-circulation is preferred over wet re-circulation. However, dry re-circulation requires additional equipment, e.g. heat exchangers for cooling, condensing and re-heating processes, which should be energetically integrated into the overall process. A future assessment should also be made to

see if the improvement in combustion efficiency resulting from dry re-circulation compared to wet re-circulation offsets the efforts required, both in economic and energetic terms. In addition, small differences were found depending on whether the steam flow to the fuel reactor was maintained because the majority of the steam flow comes from the carbon stripper.

3.3.2. D-3B: Recycling exhaust gas to the carbon stripper

The *i*G-CLC system includes another reactor to which exhaust gases could be re-circulated without sustaining losses of carbon to the air reactor: the carbon stripper. This option is called D-3B, and in this configuration unconverted gases would be oxidised by oxygen carrier inside this reactor. As in option D-3A, dry re-circulation is assumed; see Fig. 3(d) and the steam flow to the carbon stripper is also replaced by a re-circulated flow, $F_{rec,dry}$. Steam consumption for the carbon stripper is therefore avoided. In this particular configuration, steam is used to fluidise the fuel reactor. The carbon stripper operates in bubbling fluidisation mode to minimise oxygen carrier entrainment while char separation is carried out. The gas velocity is fixed to enhance the char separation from the oxygen carrier since lighter char particles are selectively elutriated. This fact is related to the ratio between the gas velocity in the carbon stripper ($u_{g,CS}$ = 0.25 m/s) and the estimated terminal velocity of oxygen carrier particles ($u_{t,OC}$ = 1.7 m/s) and char particles ($u_{t,char}$ = 0.18 m/s). Therefore, the re-circulated gas flow is set at being equal to the value of the steam flow for the design conditions, i.e. $F_{rec,dry}$ = 213 Nm^3/h, for a correct operation of the carbon stripper. The corresponding gas re-circulation ratio, $\phi_{g,dry}$, is 0.76.

To model the carbon stripper, the mathematical model for the fuel reactor was modified to take into account the reactor as a bubbling fluidised bed. The fluid dynamic section of the model [34] is therefore substituted by a fluid dynamic model in bubbling mode, as described in a previous study [45]. Because gas velocity is greater than terminal velocity for char particles, the transport phase for char particles is maintained, as was the case in the model developed for the fuel reactor [34]. The model also takes into account chemical processes occurring in the carbon stripper, such as char gasification and the conversion of both gases in the re-circulated stream and gasification products owing to a reaction with the oxygen carrier. These chemical reactions are modelled in a similar way to those in the fuel reactor.

The char flow segregated from the oxygen carrier particles is calculated by using the previously defined carbon separation efficiency of the carbon stripper, η_{CS} = 99%.

Predictions made using the model show that oxygen demand and CO_2 capture efficiency for the post-combustion PC-1 option are Ω_T = 3.0% and η_{CC} = 95.5%, respectively. In this case, oxygen demand is significantly less than $\Omega_{T,ref}$ = 11.4% in the reference case, whereas the CO_2 capture is slightly affected in comparison ($\eta_{CC,ref}$ = 96.4%): a lower CO_2 capture is predicted because of the lower steam concentration in the fuel reactor when steam is replaced by re-circulated gases. Here it is important to note that steam acts as a gasifying agent. If the post-combustion PC-2 option is chosen, the CO_2 capture efficiency increases from 89.7% in the reference case to 92.3% with gas recycling to the carbon stripper.

3.4. D-4: Recycling unburnt gases to the fuel reactor after CO_2 separation

In this option, unburnt gases from the GPU unit are recycled to the fuel reactor, see Fig. 3(e). For preliminary estimations, it is assumed that an ideal CO_2 separation is reached inside the GPU unit, i.e. the compressed CO_2 stream only contains CO_2, whereas there is no CO_2 in the stream of incondensable gases, which contains unburnt products and nitrogen. Nitrogen coming from the fuel is expected to be mainly N_2 [43]. In this option, there is no oxygen demand because the oxygen polishing step is not required.

To avoid N_2 accumulation in the system, a purge stream is required, which can then be sent to the air reactor. The purge stream must contain a nitrogen flow (based on N atoms) equal to the nitrogen flow contained in the coal fed (N_2 intrusion from air is not expected). To fulfil this requirement, the purge stream is approximately half of the incondensable flow gas reaching the GPU. If an oxygen polishing step was applied to this stream, i.e. the PC-1 option, oxygen demand would be 6.6% and CO_2 capture efficiency 96.4%. Nevertheless, it is intended that the purge stream should go to the air reactor, where unconverted compounds will be burnt by air. This case is similar to the post-combustion PC-2 option and some carbon will be lost as CO_2 from the air reactor. The CO_2 capture efficiency therefore decreases from 96.4%, in the reference case, to 92.5%.

3.5. D-5:Feeding coal into the carbon stripper

In this case, the carbon stripper acts also as the primary fuel reactor, and the fuel reactor is the secondary fuel reactor, see Fig. 3(f). The carbon stripper is fluidised by steam operating in bubbling mode. Volatile matter and gasification products generated in the carbon stripper are partially burnt in the carbon stripper. Gases from the carbon stripper subsequently go to the fuel reactor together with char particles entrained from the bed. In the fuel reactor, further oxidation of volatile matter and gasification products occurs, as well as the gasification of solid carbon. Char particles are therefore continuously circulating between the carbon stripper and the fuel reactor until complete gasification is achieved or these are bypassed to the air reactor.

Modifications to the carbon stripper model include adding two steams containing carbon solids to the inlet stream, i.e. coal and re-circulated char, and the generation of volatile matter. As in the fuel reactor model, coal devolatilisation is assumed to happen instantaneously at the feeding point. This situation is similar to the fuel reactor for the reference case, but the carbon stripper is a bubbling fluidised bed. Also, the solid fuel fed into the fuel reactor is simply char coming from the carbon stripper, similar to the carbon stripper in the reference case. Thus, the carbon stripper and the fuel reactor models are executed alternatively. The solution is reached by means of an iterative process, whereby input data for the fuel reactor model comes from the output results of the carbon stripper, and *vice versa*.

When coal is fed into the carbon stripper, the carbon load to the carbon stripper is increased because the carbon in coal is added to the carbon in the char coming from the fuel reactor. As a consequence, the CO_2 capture efficiency decreases slightly to η_{CC} = 96.0% in PC-1 option if the efficiency of carbon separation is assumed to be equal to that cited in the reference case, i.e. η_{CS} = 99%. Note that the mathematical model predicts that only 0.03 wt.% of solids in the carbon stripper are char particles, which can be compared to the 0.5 wt.% predicted in the fuel reactor. This means that most of the char gasification takes place in the fuel reactor. Only 2.8% of char is predicted to be gasified in the carbon stripper. In the case of post-combustion option PC-2, CO_2 capture is 92.7%, a figure that is significantly higher than that obtained in the reference case ($\eta_{CC,ref}$ = 89.7%).

More significant, however, is the decrease in the oxygen demand, which reached a value of Ω_T = 5.8%. This is owing to the fact that volatile matter is oxidised by a higher amount of solids present in both the carbon stripper and the fuel reactor. If methane is considered as a representative compound in the volatile matter, the flow of methane exiting the carbon stripper is $2.3 \cdot 10^{-2}$ mol/s, whereas the methane flow decreases to $5.8 \cdot 10^{-3}$ mol/s after the fuel reactor. However, the oxygen demand at the carbon stripper exit is 4.8%, which is lower than after the fuel reactor. The higher oxygen demand predicted after the fuel reactor is due to the accumulation of gasification products, i.e. H_2 and CO, in the freeboard of the fuel reactor. This means that more gasification products are generated than those oxidised by the reaction with ilmenite.

4. Discussion

4.1. Comparison of different options

Different options have been analysed in order to reduce or avoid the oxygen requirements in an oxygen polishing step due to unconverted gases present together with the CO_2 stream coming from the fuel reactor in an *i*G-CLC system. A summary of the oxygen demand and the CO_2 capture efficiency obtained for every option is shown in Table 4. This table also shows the gas flow and the composition of the stream reaching the post-combustion system; see Fig. 4. The gas flow and composition could be used to evaluate the energy efficiency of the *i*G-CLC system [10].

High oxygen demand reductions are predicted for all cases; however, complete combustion is not reached. All the options do not have the same impact on reducing the oxygen demand. To compare the effect of the different options on the oxygen demand and the CO_2 capture efficiency, the coefficient of variation, *CV*, of the parameter *x* is defined as:

$$CV(\%) = 100 \frac{x_{new} - x_{ref}}{x_{ref}} \quad (19)$$

with x_{ref} being the oxygen demand or the CO_2 capture efficiency for the reference case, and x_{new} being the value of these parameters for an option in question. The coefficient of variation for the oxygen

demand and the CO_2 capture for the options evaluated in this paper are shown in Fig. 7 for the post-combustion PC-1 option. In all cases, the effect on the CO_2 capture is low, although some reduction in η_{CC} is observed, mainly for options D-1 and D-3B.

Table 4. Summary of predictions for the different technological options evaluated in this work.

	Reference	D-1	D-2	D-3A	D-3B	D-4	D-5	D-6
m_{FR-1} (kg)	380	380	380	380	380	380	380	380
m_{FR-2} (kg)	-	-	190	-	-	-	-	-
m_{CS} (kg)	510	510	510	510	510	510	510	510
m_{total} (kg)	890	890	1080	890	890	890	890	890
m_{total} (kg/MW_{th})	2320	2320	2800	2320	2320	2320	2320	2320
Option PC-1								
Ω_T (%)	11.4	7.5	1.7	3.7	3.0	6.6	5.8	0.9
η_{CC} (%)	96.4	95.1	96.4	97.1	95.5	96.4	96.0	98.8
Option PC-2								
Ω_T (%)	0	0	0	0	0	0	0	0
η_{CC} (%)	89.7	90.7	95.4	92.2	92.3	92.5	92.7	98.4
Gas flow (mol/h)	4.85	4.87	4.88	1.44	1.17	4.97	4.91	2.68
Gas composition (%)								
CO_2	15.68	15.81	16.57	54.34	66.74	15.80	16.00	31.10
H_2O	80.86	81.59	83.05	41.06	28.73	80.28	80.78	68.35
CH_4	0.49	0.23	0.17	0.42	0.45	0.59	0.12	0.16
CO	0.68	0.53	0.00	2.41	1.81	0.73	0.47	0.00
H_2	2.08	1.63	0.01	1.08	1.44	2.20	1.43	0.01
N_2	0.15	0.15	0.14	0.49	0.59	0.28	0.15	0.27
SO_2	0.06	0.06	0.06	0.20	0.25	0.12	0.06	0.11

The effect of the design option chosen on the oxygen demand is more important. The highest reduction in oxygen demand was observed for option D-2, i.e. the implementation of a secondary fuel reactor. Nevertheless, this option involves operating four interconnected fluidised bed reactors, which increases the complexity of the reactor integration, and also requires a higher amount of oxygen carrier material.

Gas re-circulation to the fuel reactor or the carbon stripper also shows a high reduction in the oxygen demand values. In these cases, the gas flow inside the fuel reactor could be higher than in the reference case, which affects the fluid dynamics of the reactor. Here it must be highlighted that the gas flow

reaching the post-combustion and GPU stages is lower because the steam flow is replaced by re-circulated gas. This fact could be beneficial for the efficiency of the process because the energetic penalty linked to steam generation is reduced.

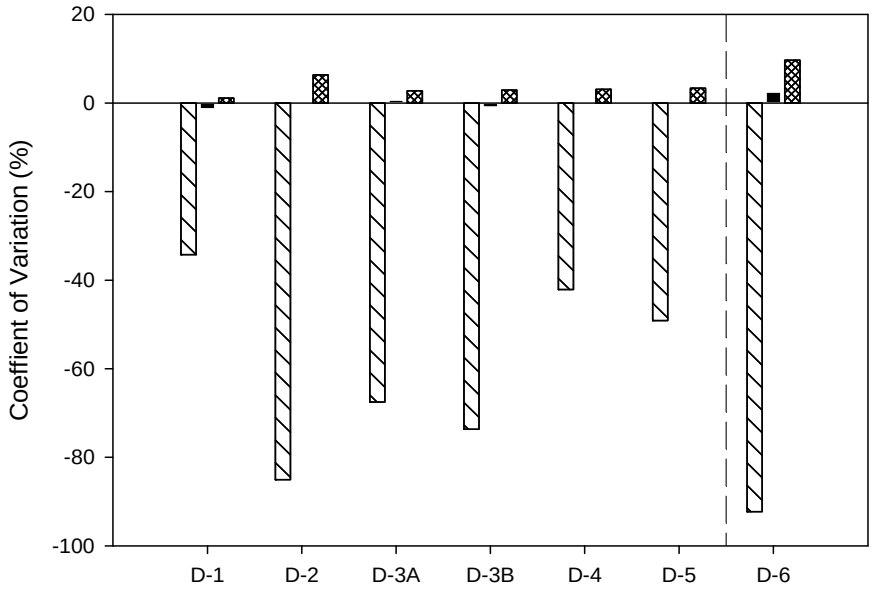

Fig. 7. Coefficient of variation, *CV*, for the oxygen demand and CO_2 capture predicted for the technological options evaluated in this work. Post-combustion options PC-1: oxygen demand ; CO_2 capture efficiency . Post-combustion options PC-2: CO_2 capture efficiency .

Some considerations may be made with respect to the re-circulation of gases to the fuel reactor or the carbon stripper. Re-circulating gas to the carbon stripper (D-3B) leads to a higher reduction in oxygen demand than re-circulation to the fuel reactor (D-3A); however, it must be noted that the carbon capture efficiency is lower in option D-3B. At this point, the option of re-circulating gas to both the fuel reactor and the carbon stripper simultaneously can be introduced. In this case, the use of steam would be avoided, leading to improved plant efficiency. Similar results are obtained in this option, although the carbon capture is lower than the level obtained through option D-3B because of the scarce steam availability for char gasification. The option of introducing wet coal to generate steam into the fuel reactor could be explored in the future.

Similarities are found between options D-3B and D-2. In both cases, unconverted compounds exiting the fuel reactor are burnt in a downstream reactor. In option D-2, all the gas has the chance to react in a secondary reactor, whereas in option D-3B only re-circulated gases are able to react in the carbon stripper. The solids inventory in the carbon stripper was about 1300 kg/MW_{th}, and the oxygen demand for option D-3B was 3.0%. However, the solids inventory in the secondary reactor for option D-2 was 500 kg/MW_{th}, whereas the oxygen demand was Ω_T = 1.7%; see Table 4. Thus, a lower oxygen demand is obtained in option D-2, even with a lower solids inventory in the downstream reactor. Incomplete inherent combustion associated to the re-circulation concept (D-3B) prevents a lower oxygen demand than in the option D-2. However, option D-2 does not exclude the presence of the carbon stripper. Thus, the use of option D-2 must always be considered with a higher amount of solids in the *i*G-CLC system than option D-3B.

Feeding coal into the carbon stripper, option D-5, also leads to a relatively high reduction in oxygen demand. In this case, the conceptual design of the *i*G-CLC system is different. On the one hand, the carbon stripper acts as a primary fuel reactor, and char particles are separated from oxygen carrier particles, which prevents a high extension of gasification in this reactor. On the other hand, the existing fuel reactor, as in Fig. 1, can be considered as a secondary fuel reactor. In this latter reactor, the oxidation of gases coming from the carbon stripper occurs together with the large part of the char gasification in the *i*G-CLC system. In fact, an accumulation of gasification products in the freeboard prevents a higher fall in oxygen demand.

If post-combustion option PC-2 is chosen, the oxygen polishing step is avoided. However, CO_2 capture values lower than 95% are obtained in most cases. In this sense, post-combustion option PC-1 with an oxygen polishing step would be preferred, as previously suggested by other authors [10]. Nevertheless, option D-2 was the only design option with CO_2 capture efficiency values higher than 95%, which is similar to the values obtained for option PC-1. Thus, post-combustion option PC-2 can be viewed as a feasible alternative to deal with unconverted gases in design option D-2.

One way to reduce the presence of unburnt products in the CO_2 stream could be to include combinations of the options analysed above. For example, it would be feasible to implement geometrical restrictions

in the fuel reactor as well as to include a secondary reactor in the *i*G-CLC system. This option merges options D-1 and D-2, and allows oxygen demand to reach a value as low as 0.8%. The main unconverted product is CH_4 from volatile matter because of the low reactivity of this gas with ilmenite. The use of a more reactive oxygen carrier material would allow the oxygen demand in the process to be minimised.

From the above considerations, the following conclusions can be drawn:

- The fuel reactor partially converts volatile matter, and most of the char is gasified there.
- The carbon stripper must be designed in order to have a high efficiency of carbon separation from the oxygen carrier particles. Moreover, the carbon stripper operates with a low fraction of char particles in the solids. This fact means that gasification products are accumulated in the reactor and relatively good combustion is achieved in this reactor, as shown in the results from option D-3B.
- In this process, CH_4, CO and H_2 are unconverted gases. Two categories have been identified: CH_4 that comes mainly from volatile matter because the low reactivity of ilmenite with this gas; and CO and H_2 that mainly come from the accumulation of gasification products in the freeboard. Thus, CO and H_2 are the main unconverted gases exiting the fuel reactor, where char gasification mainly occurs. In the carbon stripper, where gasification is of lower significance, or the secondary fuel reactor, where there is no char, the gasification products are deeply converted.

4.2. Proposal of a new iG-CLC arrangement

Based on these considerations, a new concept for the reactor arrangement is proposed. The proposed *i*G-CLC concept is shown in Fig. 8 and referred to as design option D-6. Coal is fed into the fuel reactor, where it is devolatilised and gasified by steam or CO_2 in the fluidisation gas. Volatile matter and gasification products are partially converted to CO_2 and H_2O, with CH_4, CO and H_2 being present in the product gas. Solids are transported to the carbon stripper. To improve the CO_2 capture, it is desirable to take solids from the bottom bed because the char concentration is lower than in the freeboard [34] in this zone. In addition, the carbon stripper is fluidised by hot gases coming from the fuel reactor. No steam condensation is required in this step. Thus, the carbon stripper also acts as a secondary fuel reactor. To maintain the fluid dynamic properties of the carbon stripper as equal to those in the reference case,

steam must be added to the carbon stripper to reach a total flow of gas in the carbon stripper of 213 Nm^3/h; see Table 3. Therefore, the total steam requirement in both the fuel reactor and carbon stripper is reduced to 110 Nm^3/h, instead of 290 Nm^3/h as cited in the reference case. Solids elutriated from the carbon stripper are concentrated in the char, being re-circulated to the fuel reactor. The efficiency of the carbon stripper is assumed to be equal to η_{CS} = 99%. Thus, only 1% of char particles reaching the carbon stripper are left to pass to the air reactor, where they will be burnt with air. Most char particles are continuously re-circulated between the fuel reactor and the carbon stripper. Char is concentrated in the fuel reactor, where 99.1% of carbon is gasified. Only 0.9% of carbon is gasified in the carbon stripper. The gas stream exiting the carbon stripper contains the desired highly pure CO_2, which is sent to the post-combustion or GPU unit.

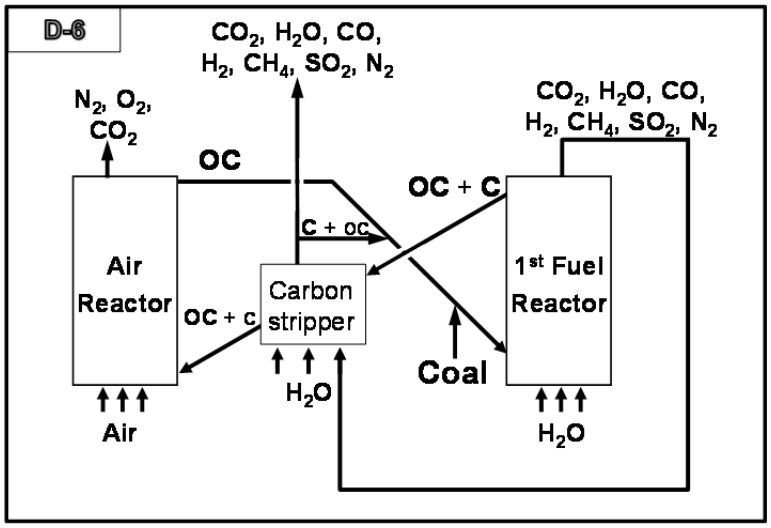

Fig. 8. General flow sheet for the improved *i*G-CLC concept proposed in this work.

The gas flow and concentration of gaseous species in this stream is shown in Table 4. Special mention must be made of the low fraction of CH_4 and the absence of gasification products, in line with the good performance of the carbon stripper as a secondary fuel reactor and the low fraction of char gasified there. Oxygen demand falls to a low value of Ω_T = 0.9%, whereas CO_2 capture is η_{CC} = 98.8%. In this case, the post-combustion option PC-2 could be a good option from an energetic point of view because

of the low fraction of incondensable gases. In this case, the predicted CO_2 capture is η_{CC} = 98.4%. This new *i*G-CLC concept may be implemented with just a few changes to the original system, and it has major potential to increase the combustion efficiency in the system, and to even increase the CO_2 capture efficiency over and above the numbers predicted for other design options analysed in this paper.

5. Conclusions

Several design options have been evaluated in order to reduce the presence of unburnt compounds together with the CO_2 stream in the *in-situ* gasification chemical looping combustion (*i*G-CLC) process. A mathematical model previously validated against experimental results was conveniently modified to consider the proposed design options, which include increasing the gas-solid contact in the fuel reactor, incorporating a secondary fuel reactor, re-circulating exhaust gases to the fuel reactor or the carbon stripper, or feeding coal into the carbon stripper instead of into the fuel reactor. The highest reduction in the oxygen demand was predicted for the option involving the use of a secondary fuel reactor. Based on these findings, an *i*G-CLC concept with a new reactor configuration is proposed. This new concept sends exhaust gases from the fuel reactor to the carbon stripper. Most of the char is gasified in the fuel reactor, and the carbon stripper also acts as a secondary fuel reactor. The oxygen demand for this concept is predicted to be Ω_T = 0.9% and the CO_2 capture efficiency is η_{CC} = 98.8%. If incondensable gases were separated in the GPU and sent to the air reactor, the oxygen polishing would be avoided, and the predicted CO_2 capture efficiency was η_{CC} = 98.4%.

Acknowledgements

This paper was partially supported by the European Commission, under the RFCS program (ACCLAIM Project, Contract RFCP-CT-2012-00006), the Government of Aragon and La Caixa (2012-GA-LC-076 project) and the Spanish Ministry for Science and Innovation via the ENE2010-19550 project.

Submitted, accepted and published by
Chemical Engineering Journal 233 (2013) 56–69

Nomenclature

a	decay constant for solids in the splash phase
C_b	solids concentration in the bottom bed (kg/m^3)
C_{spl}	solids concentration in the splash phase (kg/m^3)
C_{tr}	solids concentration in the transport phase (kg/m^3)
CV	coefficient of variation (%)
d_p	particle diameter (m)
f_C	carbon content in the coal
$f_{C,fix}$	fixed carbon of the coal
f_S	multiplying factor of solids concentration
F_i	molar flow of gas I (mol/s)
$F_{rec,dry}$	dry flow of re-circulated gases (mol/s)
$F_{outFR,dry}$	dry flow of gases exiting the fuel reactor (mol/s)
g	gravity acceleration (m/s^2)
H	height (m)
H_b	height of the bottom bed (m)
K	decay constant for solids in the transport phase
m	mass of solids (kg)
$\dot{m}_{coal}$	coal feeding rate (kg/s)
$\dot{m}_{OC}$	solids circulation flow rate (kg/s)
M_C	atomic weight of carbon ($12 \cdot 10^{-3}$ kg/mol)
M_O	atomic weight of oxygen ($16 \cdot 10^{-3}$ kg/mol)
n_{int}	number of internals
R_{OC}	oxygen transport capacity (kg oxygen per kg of oxygen carrier)
u_g	gas velocity (m/s)
u_t	terminal velocity (m/s)
x_{new}	parametric value newly evaluated
x_{ref}	parametric value for the reference case
z	axial position (m)
z_i	axial position of the internal i (m)
z^-	axial position just below the geometrical constriction (m)
z^+	axial position just above the geometrical constriction (m)

Greek symbols

Δh_{int}	separation distance between internals (m)
ΔP	pressure drop in the reactor (Pa)

1	$\phi_{g,dry}$	re-circulation ratio in dry basis
2	ϕ_{OC}	oxygen carrier to fuel ratio
3	η_{CC}	CO_2 capture efficiency
4	η_{CS}	carbon separation efficiency in the carbon stripper
5	ρ_p	particle density (kg/m^3)
6	Ω_{coal}	oxygen demand of coal (kg oxygen per kg coal)
7	Ω_T	total oxygen demand of gases exiting the CLC unit
8		
9	Acronyms	
10	FR	fuel reactor
11	FR-1	primary fuel reactor
12	FR-2	secondary fuel reactor
13	AR	air reactor
14	CS	carbon stripper
15		

16

References

[1] K. Thambimuthu, M. Soltanieh, J.C. Abanades, Capture of CO_2, in: B. Metz, O. Davidson, H.C. de Coninck, M. Loos, L.A. Meyer (Eds.), IPCC Special Report on Carbon Dioxide Capture and Storage, Cambridge University Press, Cambridge, United Kingdom and New York, 2005, 105-178.

[2] J. Adanez, A. Abad, F. Garcia-Labiano, P. Gayan, L.F. de Diego, Progress in Chemical-Looping Combustion and Reforming technologies, Prog. En. Comb. Sci. 38 (2012) 215-282.

[3] M. Orth, J. Ströhle, B. Epple, Design and Operation of a 1 MW_{th} Chemical Looping Plant, Proc. 2nd Int. Conf. Chemical Looping, Darmstadt, Germany, 2012.

[4] L. Shen, J. Wu, J. Xiao, Experiments on chemical looping combustion of coal with a NiO based oxygen carrier, Comb. Flame 156 (2009) 721-728.

[5] A. Thon, M. Kramp, E.-U. Hartge, S. Heinrich, J. Werther, Operational experience with a coupled fluidized bed system for chemical looping combustion of solid fuels, Proc. 2nd Int. Conf. Chemical Looping, Darmstadt, Germany, 2012.

[6] N. Berguerand, A. Lyngfelt, Design and operation of a 10 kW_{th} chemical-looping combustor for solid fuels - Testing with South African coal, Fuel 87 (2008) 2713-2726.

[7] P. Markström, C. Linderholm, A. Lyngfelt, Chemical-looping combustion of solid fuels – Design and operation of a 100 kW unit with bituminous coal, Int. J. Greenhouse Gas Control 15 (2013) 150-162.

[8] T. Sozinho, W. Pelletant, H. Stainton, F. Guillou, T. Gauthier, Main results of the 10 kW_{th} pilot plant operation, Proc. 2nd Int. Conf. Chemical Looping, Darmstadt, Germany, 2012.

[9] Y. Cao, W.-P. Pan, Investigation of Chemical Looping Combustion by Solid Fuels. 1. Process Analysis, Energy Fuels 20 (2006) 1836-1844.

[10] V. Kempkes, A. Kather, Chemical Looping Combustion: Comparative Analysis of two Different Overall Process Configurations for Removing Unburnt Gaseous Components, Proc. 2nd Int. Conf. Chemical Looping, Darmstadt, Germany, 2012.

[11] A. Cuadrat, C. Linderholm, A. Abad, A. Lyngfelt, J. Adánez, Influence of Limestone Addition in a 10 kW_{th} Chemical-Looping Combustion Unit Operated with Petcoke, Energy Fuels 25 (2011) 4818-4828.

[12] N. Berguerand, A. Lyngfelt, The use of petroleum coke as fuel in a 10 kW_{th} chemical-looping combustor, Int. J. Greenhouse Gas Control 2 (2008) 169-179.

[13] N. Berguerand, A. Lyngfelt, Chemical-Looping Combustion of Petroleum Coke Using Ilmenite in a 10 kW_{th} Unit - High-Temperature Operation, Energy Fuels 23 (2009) 5257-5268.

[14] A. Cuadrat, A. Abad, F. García-Labiano, P. Gayán, L.F. de Diego, J. Adánez, Relevance of the coal rank on the performance of the in situ gasification chemical-looping combustion, Chemical Engineering Journal 195-196 (2012) 91-102.

[15] A. Cuadrat, A. Abad, F. García-Labiano, P. Gayán, L.F. de Diego, J. Adánez, The use of ilmenite as oxygen-carrier in a 500 W_{th} Chemical-Looping Coal Combustion unit, Int. J. Greenhouse Gas Control 5 (2011) 1630-1642.

[16] A. Cuadrat, A. Abad, F. García-Labiano, P. Gayán, L.F. de Diego, J. Adánez, Effect of operating conditions in Chemical-Looping Combustion of coal in a 500 W_{th} unit, Int. J. Greenhouse Gas Control 6 (2012) 153-163.

[17] C. Linderholm, A. Lyngfelt, A. Cuadrat, E. Jerndal, Chemical-looping combustion of solid fuels - Operation in a 10 kW unit with two fuels, above-bed and in-bed fuel feed and two oxygen carriers, manganese ore and ilmenite, Fuel 102 (2012) 808-822.

[18] A. Abad, J. Adánez, L.F. de Diego, P. Gayán, F. García-Labiano, A. Lyngfelt, Fuel reactor model validation: assessment of the key parameters affecting the chemical-looping coal combustion process, submitted for publication.

[19] P. Markström, C. Linderholm, A. Lyngfelt, Operation of a 100 kW chemical-looping combustion with Mexican petroleum coke and Cerrejón coal, Proc. 2nd Int. Conf. Chemical Looping, Darmstadt, Germany, 2012.

[20] L. Shen, J. Wu, J. Xiao, Q. Song, R. Xiao, Chemical-Looping Combustion of Biomass in a 10 kW_{th} Reactor with Iron Oxide As an Oxygen Carrier, Energy Fuels 23 (2009) 2498-2505.

[21] T. Mendiara, A. Abad, L.F., de Diego, F. García-Labiano, P. Gayán, J. Adánez, Biomass combustion in a CLC system using an iron ore as oxygen carrier, Submitted for publication (2013).

[22] T. Song, L. Shen, H. Zhang, H. Gu, S. Zhang, J. Xiao, Chemical looping combustion of two bituminous coal/char with natural hematite as oxygen carrier in 1 kW_{th} reactor, Proc. 2nd Int. Conf. Chemical Looping, Darmstadt, Germany, 2012.

[23] T. Song, T. Shen, L. Shen, J. Xiao, H. Gu, S. Zhang, Evaluation of hematite oxygen carrier in chemical-looping combustion of coal, Fuel 104 (2013) 244-252.

[24] R. Xiao, L. Chen, C. Saha, S. Zhang, S. Bhattacharya, Pressurized chemical-looping combustion of coal using an iron ore as oxygen carrier in a pilot-scale unit, Int. J. Greenhouse Gas Control 10 (2012) 363-373.

[25] T. Mendiara, L.F. de Diego, F. García-Labiano, P. Gayán, A. Abad, J. Adánez, Behaviour of a bauxite waste material as oxygen carrier in a 500 W_{th} CLC unit with coal, Int. J. Greenhouse Gas Control 17 (2013) 170-182.

[26] T. Mendiara, M.T. Izquierdo, A. Abad, L.F. de Diego, F. García-Labiano, P. Gayán, J. Adánez, Performance of a Fe-based residue using different coals in a 500 W_{th} CLC unit, Proc. 2nd Int. Conf. Chemical Looping, Darmstadt, Germany, 2012.

[27] T. Mendiara, M.T. Izquierdo, A. Abad, P. Gayán, F. García-Labiano, L.F. de Diego, J. Adánez, Mercury speciation in coal combustion with CO_2 capture by Chemical Looping Combustion, submitted for publication (2013).

[28] L. Shen, J. Wu, Z. Gao, J. Xiao, Characterization of chemical looping combustion of coal in a 1 kW_{th} reactor with a nickel-based oxygen carrier, Comb. Flame 157 (2010) 934-942.

[29] L. Shen, J. Wu, Z. Gao, J. Xiao, Reactivity deterioration of NiO/Al_2O_3 oxygen carrier for chemical looping combustion of coal in a 10 kW_{th} reactor, Comb. Flame 156 (2009) 1377-1385.

[30] I. Adánez-Rubio, A. Abad, P. Gayán, L.F. de Diego, F. García-Labiano, J. Adánez, Biomass combustion in a CLOU process with CO_2 capture, Submitted for publication (2013).

[31] I. Adánez-Rubio, A. Abad, P. Gayán, L.F. de Diego, F. García-Labiano, J. Adánez, Performance of CLOU process in the combustion of different types of coal with CO_2 capture, Int. J. Greenhouse Gas Control 12 (2013) 430-440.

[32] A. Abad, I. Adánez-Rubio, P. Gayán, F. García-Labiano, L.F. de Diego, J. Adánez, Demonstration of chemical-looping with oxygen uncoupling (CLOU) process in a 1.5 kW_{th} continuously operating unit using a Cu-based oxygen-carrier, Int. J. Greenhouse Gas Control 6 (2012) 189-200.

[33] M. Kramp, A. Thon, E.-U. Hartge, S. Heinrich, J. Werther, Carbon Stripping – A Critical Process Step in Chemical Looping Combustion of Solid Fuels, Chem. Eng. Technol. 35 (2012) 497-507.

[34] A. Abad, P. Gayán, L.F. de Diego, F. García-Labiano, J. Adánez, Fuel reactor modelling in chemical-looping combustion of coal: 1. model formulation, Chem. Eng. Sci. 87 (2013) 277-293.

[35] F. García-Labiano, L.F. de Diego, P. Gayán, A. Abad, J. Adánez, Fuel reactor modelling in chemical-looping combustion of coal: 2 - simulation and optimization, Chem. Eng. Sci. 87 (2013) 173-182.

[36] P. Gayán, I. Adánez-Rubio, A. Abad, L.F. de Diego, F. García-Labiano, J. Adánez, Development of Cu-based oxygen carriers for Chemical-Looping with Oxygen Uncoupling (CLOU) process, Fuel 96 (2012) 226-238.

[37] I. Adánez-Rubio, A. Abad, P. Gayán, L.F. de Diego, F. García-Labiano, J. Adánez, Identification of operational regions in the Chemical-Looping with Oxygen Uncoupling (CLOU) process with a Cu-based oxygen carrier, Fuel 102 (2012) 634-645.

[38] T. Mattisson, A. Lyngfelt, H. Leion, Chemical-looping with oxygen uncoupling for combustion of solid fuels, Int. J. Greenhouse Gas Control 3 (2009) 11-19.

[39] A. Cuadrat, A. Abad, P. Gayán, L.F. de Diego, F. García-Labiano, J. Adánez, Theoretical approach on the CLC performance with solid fuels: Optimizing the solids inventory, Fuel 97 (2012) 536-551.

[40] D.C. Guío-Pérez, H. Hofbauer, T. Pröll, Effect of Ring-Type Internals on Solids Distribution in a Dual Circulating Fluidized Bed System-Cold Flow Model Study, AIChE J. (2013) doi: 10.1002/aic.14168.

[41] J.C. Schmid, T. Pröll, H. Kitzler, C. Pfeifer, H. Hofbauer, Cold flow model investigations of the countercurrent flow of a dual circulating fluidized bed gasifier, Biomass Conv. Bioref. 2 (2012) 229-244.

[42] J. Adánez, P. Gayán, L.F. de Diego, F. García-Labiano, A. Abad, Combustion of Wood Chips in a CFBC. Modeling and Validation. Ind. Eng. Chem. Res. 42 (2003) 987-999.

[43] T. Song, L. Shen, J. Xiao, D. Chen, H. Gu, S. Zhang, Nitrogen transfer of fuel-N in chemical looping combustion, Comb. Flame 159 (2012) 1286-1295.

[44] A. Abad, J. Adánez, A. Cuadrat, F. García-Labiano, P. Gayán, L.F. de Diego, Kinetics of redox reactions of ilmenite for chemical-looping combustion, Chem. Eng. Sci. 66 (2011) 689-702.

[45] A. Abad, J. Adánez, F. García-Labiano, L.F. de Diego, P. Gayán, Modeling of the chemical-looping combustion of methane using a Cu-based oxygen-carrier, Comb. Flame 157 (2010) 602-615.